BMR Journal of Australian Geology & Geophysics, 8, 35-51

DETAILED SEISMIC VELOCITY/DEPTH MODELS OF THE UPPER LITHOSPHERE OF THE PILBARA CRATON, NORTHWEST AUSTRALIA

B.J. Drummond

Detailed velocity/depth models of the crust of the Pilbara Craton have been produced from amplitude studies of refracted and reflected seismic waves and their travel-times. On three profiles, a near-surface high-velocity layer, in which the velocity sometimes reaches 6.65 km s^{-1}, is interpreted as Hamersley Basin strata overlying the crystalline basement. The seismic velocity in the near-surface crystalline basement is about 6.0 km s^{-1}, and increases with depth through the crust, reaching 6.1–6.2 km s^{-1} at 11–14 km depth. Below this, at about 15 km depth, a steeper gradient to 6.35–6.45 km s^{-1} defines an intracrustal seismic boundary. In the lower part of the crust, velocity gradients increase the velocity to 6.6–7.2 km s^{-1}. In some models, second-order velocity increases with depth are used to explain bright cusps in the data, although these could also be caused by topography on the crust/mantle boundary. The crust/mantle boundary is transitional over 4-5 km, and upper mantle (Pn) velocities range from 7.5 to 8.5 km s^{-1}. On one profile, a sub-Moho boundary at which the velocity increases from 8.2 to 8.35 km s^{-1} was recognised 14 km below the crust/mantle boundary.

Previously published seismic models of the region show lateral inhomogeneity in the crust of the Capricorn Orogenic Belt, and this complicates a quantitative analysis of the amplitudes of seismic signals recorded in the orogen. However, a qualitative analysis based on the observed amplitudes, the positions of the ray-critical cusps of the previously published models, and the gravity field suggests that, while the intracrustal boundary at about 15 km depth may be sharp, the lower crust in the orogen must have high seismic velocities (and densities) and the crustal thickness in the previous models is probably not an overestimate. Increasing metamorphic grade with depth in the Yilgarn Craton probably ensures positive velocity gradients in the crust in the craton, so that the crustal thickness in the previously published models is considered reasonable. Thus, the interpreted large difference in crustal thickness between the Pilbara Craton (approximately 30 km) and the Yilgarn Craton (50 km) is substantiated.

Introduction

Seismic velocity models of the crust of the Precambrian shield in north-west Australia published to date (Drummond, 1979a; 1981; Drummond & others, 1981) were all based on the travel times of refracted waves, and, for simplicity, were based on the assumption that discrete layers with uniform velocity exist in the crust. Such models are useful for studies of lateral structures within the crust, and can provide valuable control in studies of the tectonic processes likely to have been active during the evolution of the crust. However, the depths of the boundaries in such models may be in error if velocity gradients exist within the layers (Berry, 1971). This was recognised in the earlier studies, but the effects of velocity gradients on the depths of the seismic boundaries in the models were assumed to apply to the entire region. Thus, the relative crustal thicknesses throughout the region would not change and the assumptions made about crustal evolution based on crustal thicknesses were presumed to be correct.

Drummond (1979a, 1981) used the observed seismic velocities to suggest that the crust of the Pilbara and Yilgarn Cratons was probably of acid to intermediate chemical composition, but, in the absence of detailed velocity/depth information, was not able to fully explore the likely composition of the crust. As positive velocity gradients were likely in the lower crust (Drummond, 1979a, 1981), the density of the lower crust is probably higher than might be presumed from the existing seismic models. Drummond & Shelley (1981) suggested density layering within the crust of the Yilgarn Craton as a possible explanation for differences between the theoretical gravity effect of the existing seismic models and the observed gravity field, although not all the inconsistencies can be explained in this way.

The purpose of this paper is to examine in detail the variation of seismic velocity with depth in northwest Australia. The resulting seismic velocity/depth models are significantly different in many ways from the velocity/depth models of other regions of Australia, and therefore warrant a detailed analysis of the likely chemical composition of the crust, comparisons with younger regions of Australia, and a study of the implications for crustal evolutionary models. The results of these studies will be published separately.

The area of interest

In 1977, the Bureau of Mineral Resources, and the Research School of Earth Sciences of the Australian National University conducted a seismic refraction survey of the crust and upper mantle in the northern part of the Western Australian Precambrian Shield (Fig. 1). As the purpose of this paper is to present the results of an interpretation of seismic data, the following geological description is very brief. More detailed descriptions of the geology are given by Drummond (1979a, 1981) and Drummond & others (1981), and the references cited therein.

The Pilbara Block is the exposed part of the Pilbara Craton, which is shown by seismic modelling (Drummond, 1981), gravity patterns (Wellman, 1978; Drummond & Shelley, 1981), and inliers of Archaean basement outcrop, to extend southwards under the younger Archaean and lower Proterozoic Hamersley Basin cover. The Yilgarn Craton in the south of the survey area forms the basement of the Nabberu Basin.

The Ashburton Trough, Gascoyne Province, and Bangemall Basin lie in the Capricorn Orogenic Belt (Gee, 1979), and the predominantly sedimentary rocks of the belt mask the structural relations between the two Archaean cratons.

Quarry blasts at open-cut iron ore mines in the Pilbara Craton were used as seismic sources. They were located at Shay Gap and Sunrise Hill (A in Figure 1), Goldsworthy (G), Newman (B), Tom Price and Paraburdoo (D) and Pannawonica (F). A specially prepared blast was fired at Meekatharra (C). Portable seismic recorders were deployed along lines between the blasting centres to record the seismic energy. Their positions are shown in Figure 1, and full details of the survey were described by Drummond (1979b).

In the seismic models from the previous studies (Drummond, 1979a, 1981; Drummond & others, 1981), the crust of the Pilbara Craton is 28 km thick in the north and 33 km thick in the south, with little evidence for east/west dip on the crust/mantle boundary. The northern part of the Yilgarn Craton was interpreted as more than 50 km thick. The crust in the Capricorn Orogenic Belt is intermediate in thickness. Thus, the

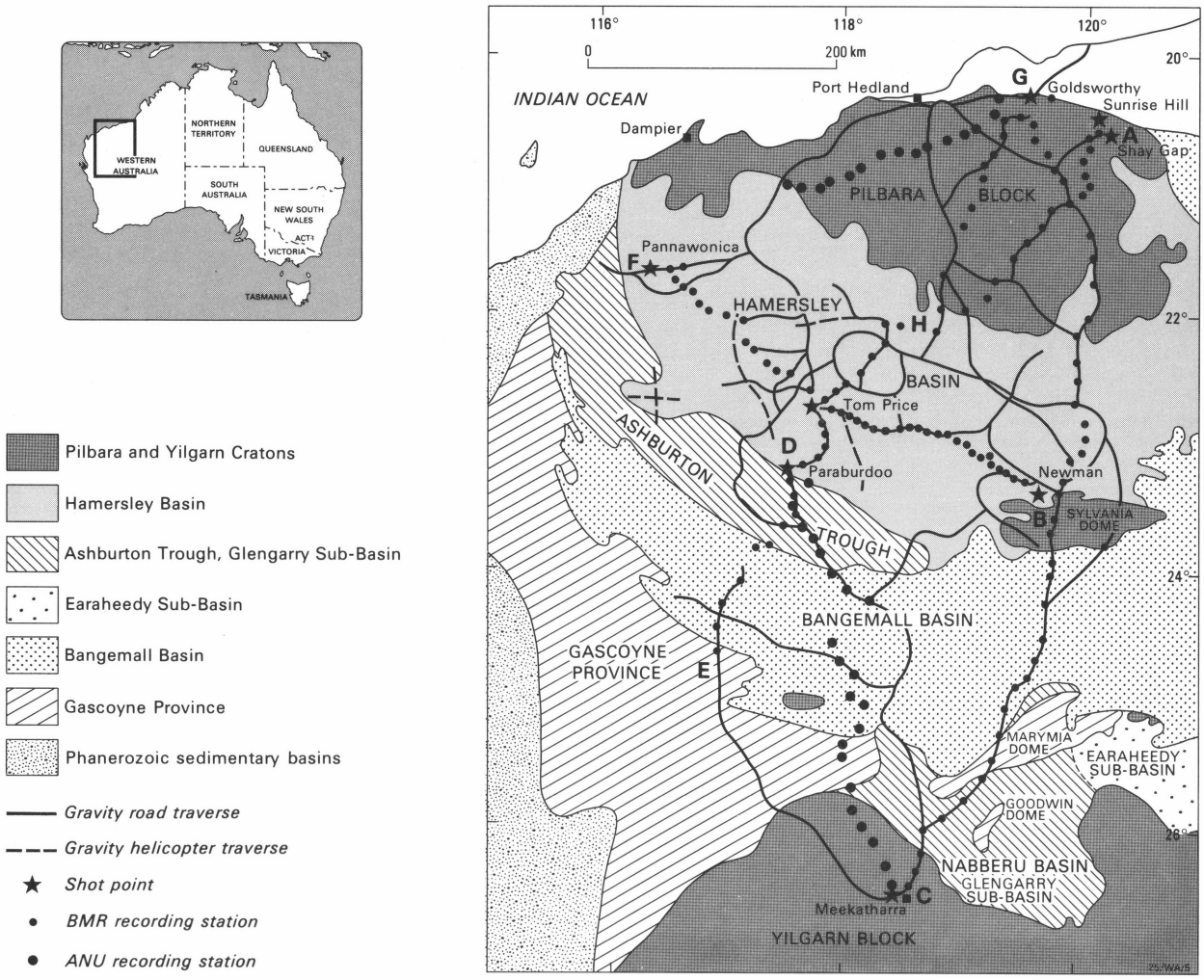

Figure 1. Geology of the survey region, and survey design.

crust in the northern part of the survey area, covering the Pilbara Craton, has little lateral structure, but across the southern part of the survey area, the depth of the crust/mantle boundary doubles, and lateral structures are significant.

Seismic modelling method

Berry (1971) emphasised the importance of recognising, and correlating between seismic traces, later arrivals that can be used to define in more detail the velocity structure with depth. He also stressed the importance of recognising and matching the position of the critical cusps. Mueller & Landisman (1971) suggested that the dynamic properties of seismic arrivals, that is, their amplitudes, phases, and frequencies, and not just their travel times, should be considered in the interpretation.

A study of the dynamic properties of seismic arrivals is inextricably linked to a study of secondary arrivals, because the secondary, wide-angle and near-critical reflections off seismic discontinuities are nearly always of higher amplitude, and therefore more easily identified, than the refracted head waves from the layers above and below the interface (Braile & Smith, 1975). However, although generally small, the amplitudes of head waves are greatly affected by velocity gradients in the refracting medium.

Amplitudes of seismic waves can be studied with the aid of synthetic seismograms. The computer program used to generate the synthetic seismograms in this study was based on the reflectivity method (Fuchs & Muller, 1971) with a modification suggested by Kind (1976) incorporated to increase the efficiency of the program. The program calculates synthetic seismograms for horizontally layered models in a flat Earth, but the models presented below (Tables 1–8; Figures 2–9) have been corrected to allow for the spherical Earth.

This synthetic seismogram technique has some limitations. Firstly, in order that phases be correctly correlated from trace to trace, Mueller & Landisman (1971) suggested that a station spacing of 3 km or less is required or phases will be missed or incorrectly correlated, a conclusion echoed by Berry & Fuchs (1973). In this study, station spacing was between 5 km near shotpoints and 25 to 30 km in the middle of some of the profiles. It is therefore possible that some travel-time branches were not recognised, or incorrect correlations made. However, within the data currently available, most of the recognised phases have been interpreted, and it seems unlikely that any major wave groups were missed.

Secondly, the computer program assumes that the Earth is composed of flat-lying, homogeneous, isotropic layers; zones of vertical velocity gradients may be represented by thin laminae of such layers (Fuchs, 1968). This is usually an over-simplification, as any geological, gravity or magnetic map will reveal. For example, in the survey area, the geological map shows several Archaean cratons, each with large, low density granitoids intruding denser greenstone belts, and separated by Proterozoic mobile belts. The first impression is, therefore, of lateral and not vertical structure. The seismic signature of flat-

lying, vertically stratified structure must, therefore, overprint that of the lateral structure before it can be accurately interpreted. As well, the effects of refractor topography can often appear to come from vertical structure (Mereu, 1969).

The use of synthetic seismograms should, therefore, be limited to regions of limited lateral structure, where a network of traverses can be used to distinguish lateral structure from vertical structure. Within the survey area, this criterion is met only within the confines of the Pilbara Craton (lines AB, FDB and GHD). Furthermore, the velocity/depth models derived below for all the seismic profiles over the Pilbara Craton by synthetic seismogram modelling are similar, and this also justifies using the technique to interpret vertical structure in the craton.

Data processing

To facilitate discussion of the velocity/depth models, their p (ray parameter) versus distance plots, and the observed and synthetic seismogram record sections, the travel-time cusps in the following discussion are annotated by the letters a, b, c, etc. The branches are:

Branch	Phase	Description of the ray path.
ab	Pg	Travels through the near-surface crystalline rocks. Along some profiles in the Hamersley Basin, some phases labelled P_1 and P_2 which travel through the basin strata are also labelled ab. The distinction is made in the text.
bc	P^I	Reflections from an intracrustal boundary.
cd	P*	Refracted below the intracrustal boundary.
de	P^M	Reflections off the crust/mantle boundary.
ef	Pn	Refractions from the uppermost mantle.
fg		Reflections off a sub-Moho boundary about 14 km below the crust/mantle boundary.
gh		Waves refracted below the sub-Moho boundary.

All data are presented in the form of record sections with a reduction velocity of 8 km s^{-1}, and were digitally bandpass filtered in the range 0.5 to 8.0 Hz. This passband removed much of the long period background noise, as well as high frequency local wind noise, while leaving the character of the principal seismic signal inviolate. When plotting the data, corrections were made for recorder gain, so that all traces in each record section are as if recorded at the same gain level.

At large distances, the geometrical spreading of head waves is proportional to distance squared, while, to a first approximation, that of reflected waves is proportional to distance (Aki & Richards, 1980). Consequently, commensurate with the expectation that the reflected waves would have the greatest amplitudes and therefore play the major role in the interpretation of amplitudes, a correction proportional to epicentral distance was applied to all data beyond the interpreted P^M/Pn cusp to account for the geometrical spreading of the wavefronts. Between the shot and about 100 km, which is about the position of the P^M/Pn critical cusp, the seismic traces were often distorted by overmodulation of the seismic channels, because of the large shot sizes. Correction of these amplitudes for geometrical spreading would have been meaningless, and, at worst, misleading. The P^M/Pn cusp was usually, though not always, characterised by large, clear and, therefore, easily recognised arrivals and was a useful datum to which the arrivals on the other traces could be related.

Braile & Smith (1975) and Berry & Fuchs (1973) also used a correction factor for geometrical spreading proportional to epicentral distance, but other workers, for example Mereu & others (1977), prefer the square of the distance. When a factor proportional to the square of the distance was used on these data, the amplitudes of the recorded signal and, especially, those of the reflected phases increased interminably with distance, which cannot happen in real data, because of natural attenuation processes and because it would imply that seismic waves could gain energy with distance from the blast.

In a few cases, additional adjustments were made to the trace amplitudes. These were generally in the form of a reduction of anomalously large amplitude arrivals, which obscured arrivals on adjacent traces and are clearly marked on the record sections by an 'X' and the reduction factor.

No amplitude corrections were made for shot weight. Many of the blasts have individual source characteristics, the differences in the waveforms being in the frequency and time duration of the signals, and not in their amplitude. No simple relationship links the observed amplitudes to the amounts of explosives used in the blasts (see also Berry & Fuchs, 1973, for similar observations of blasts specially prepared for seismic surveys). This probably stems from the practice of firing the quarrying blasts one mining bench at a time, with delays between the benches. The consequence of delays is that the amplitude of the seismic energy is related more to the quantity of explosives in each bench than the total quantity of explosives in the blast.

Synthetic seismogram modelling

Shotpoint A (Sunrise Hill & Shay Gap), along line AB

Because of the overmodulation of the near-source recordings, owing to the large quarrying blasts used for the seismic survey, very little is known about the amplitudes of the Pg phase (ab), and the P^I/P* cusp (c). Some of the smaller blasts at Shay Gap, Sunrise Hill, and Goldsworthy, however, did not overmodulate the traces, and the record section of one such blast is shown in Figure 2b. The location of the profile is shown in Figure 2a.

The Pg phase (ab) decays proportionally to a value between distance and distance squared. This implies that there is very little attenuation of the seismic energy. No upper crustal low-velocity channel similar to that found in both young and old regions elsewhere in the world (eg. Mueller & Landisman, 1966; Berry & Fuchs, 1973; Finlayson & others, 1980) can be implied. Rather, positive velocity gradients can be inferred to limit the amplitude decay to between distance and distance squared.

The amplitude of the P^I/P* cusp (c) is also further evidence that no upper crustal low-velocity channel is present in the region. Mueller & Landisman (1966) suggested that the large amplitudes of the P^I phase (bc) relative to the Pg phase (ab) in the data that they studied were evidence for a low-velocity zone; this zone brought the intracrustal boundary in their model closer to the surface, and moved the P^I/P* cusp closer to the blast. In the record section in Figure 2b, the arrowed P^I arrivals in each trace have about twice the amplitude of the Pg phase in that trace. However, the full interpretation of the P^I/P* cusp (c) cannot be made without comparing it to the P^M/Pn cusp (e). Between about 80 and 120 km, the arrivals of the P^I/P* cusp have about one-third to one-quarter the amplitude of those near the P^M/Pn cusp (e).

The P^M/Pn cusp is shown again in the record section of a different blast in Figure 2e, the location of which is shown in Figure 2d. Figure 2e also shows seismic traces beyond 200 km.

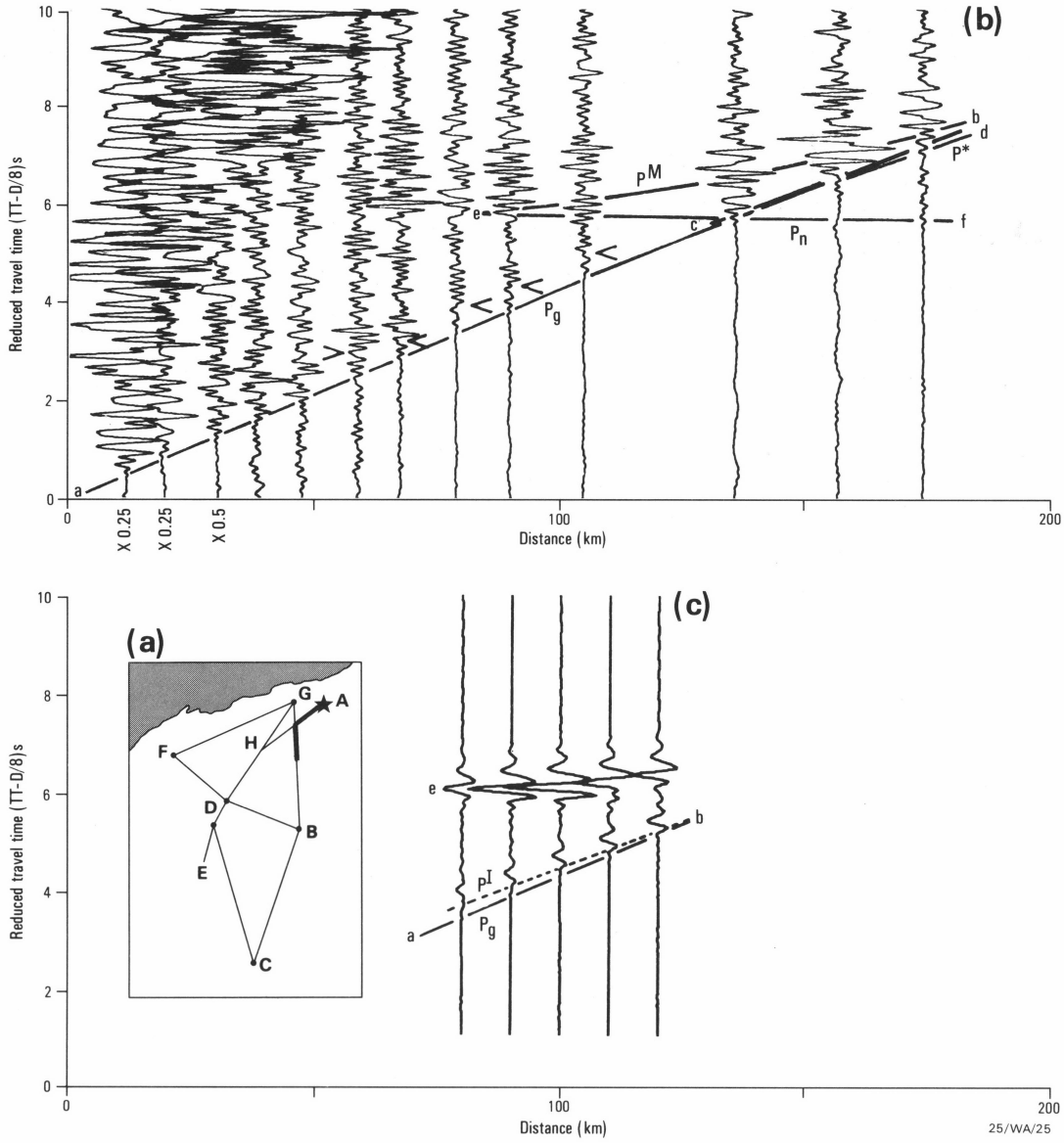

Figure 2. Model for shotpoint A (Sunrise Hill and Shay Gap), along line AB.
(a) location diagram for the record section in Figure 2b; (b) record section southwards from A. The superimposed travel-time curves are for the model in Figure 2f; (c) synthetic seismogram record section and travel-time plot for the model in Figure 2f, but with the Pg phase omitted; (d) location diagram for the record section in Figure 2e; (e) record section southwards from A. The superimposed travel-time curves are for the model in Figure 2f; (f) velocity/depth model for the profile AB; (g) p-versus-distance plot for the model in Figure 2f; (h) synthetic seismogram record section and travel-time plot for the model in Figure 2(f).

In this figure, the P^I cusp (c) is difficult to define, because the arrivals have a much lower frequency than those in Figure 2b, and are difficult to distinguish from the weak Pg phase (ab). The amplitudes of the interpreted P^I phase (arrowed) are very small compared to the amplitudes of the P^M/Pn cusp (e). The velocity/depth function derived from these record sections therefore had to model the amplitudes of the P^I/P* cusp (c) relative to the Pg phase, as well as its amplitudes relative to the P^M/Pn cusp (e). The amplitudes of the cusp at e are more easily defined than those of the Pg phase (ab). Therefore, most emphasis was placed on the comparison of the P^I/P* cusp (c) with the P^M/Pn cusp (e). The resulting model does, however, give a fair match of the amplitudes of the Pg phase and the P^I phase.

The proposed model for profile AB is shown in Figure 2f and listed in Table 1; the ray parameter (p) versus distance plot is shown in Figure 2g. The travel time curves for the model, derived by ray tracing through the model, are superimposed on the record sections in Figures 2b and 2e. The synthetic seismogram record sections, with superimposed travel-time curves, are illustrated in Figures 2c and 2h. In the synthetic seismograms of Figure 2c, the Pg phase was omitted because, as can be seen in the synthetic seismograms of Figure 2h, which contains the Pg phase, the Pg and P^I phases constructively interfere at the frequencies of the wavelet used in the synthetic seismogram modelling, and no meaningful comparison of the P^I and P^M phases can be made. The

Table 1. Velocity/depth model for the profile shotpoint A (Sunrise Hill and Shay Gap), along line AB

Velocity (km s^{-1})	*Depth (km)*	*Travel-time curve cusps*
5.95	0.0	a
6.15	11.0	b
6.25	13.0	c
6.60	28.0	d
8.20	31.0	e
8.25	42.0	f

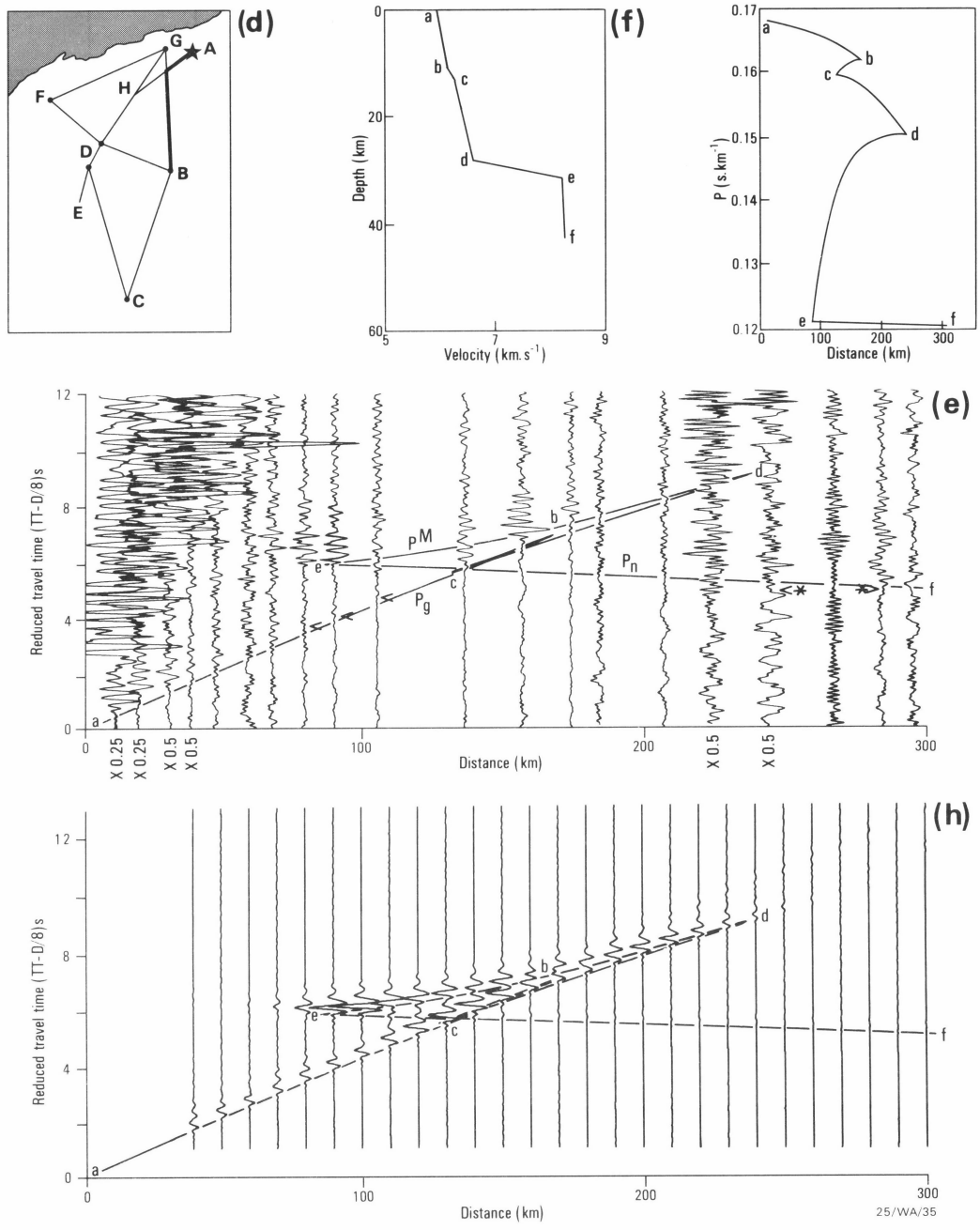

comparison can be made in Figure 2c, where the ratio of the phases' amplitudes is about one-third to one-quarter, as noted previously in the recorded data in Figure 2b.

The amplitudes of the P^I/P^* cusp (c) were reduced relative to those of the P^M/Pn cusp (e) by (1) including velocity gradients above and below the intracrustal boundary, thus forcing energy that would otherwise fall on the reflection branch onto the forward (refraction) branches either side of the reflection branch, and (2) making the boundary gradational, thereby forcing the ray-theoretical cusp further from the blast. Without the gradients above and below the boundary, and with a sharper boundary, the amplitudes of the P^I/P^* cusp (c) were too large compared to the P^M/Pn cusp (e). The intracrustal boundary creates a small triplication in the travel-time curve, and the arrowed P^I phases in Figures 2b and 2e are assumed to be subcritical reflections.

Several arrivals that could be part of the forward Pg/P^I cusp (b) can be interpreted in Figure 2e, but no convincing correlations can be made. The arrivals are generally small. The model gives a correspondingly small cusp at b (Fig. 2h).

The P^M phase weakens beyond about 180 km in the data and beyond about 200 km in the synthetic record section. Note that the Pn phase is weak in the data, although some arrivals (arrowed, with an asterisk in Figure 2e) can be interpreted. This is an important factor in the interpretation of the data from shotpoint G at Goldsworthy along line GBC.

Shotpoint G (Goldsworthy), along line GBC
(Fig. 3, Table 2)

The Pg phase (ab) has large, often overmodulated arrivals out to the crossover distance with Pn, and the arrivals at cusp e in the distance range 90 to 100 km are overmodulated. Conse-

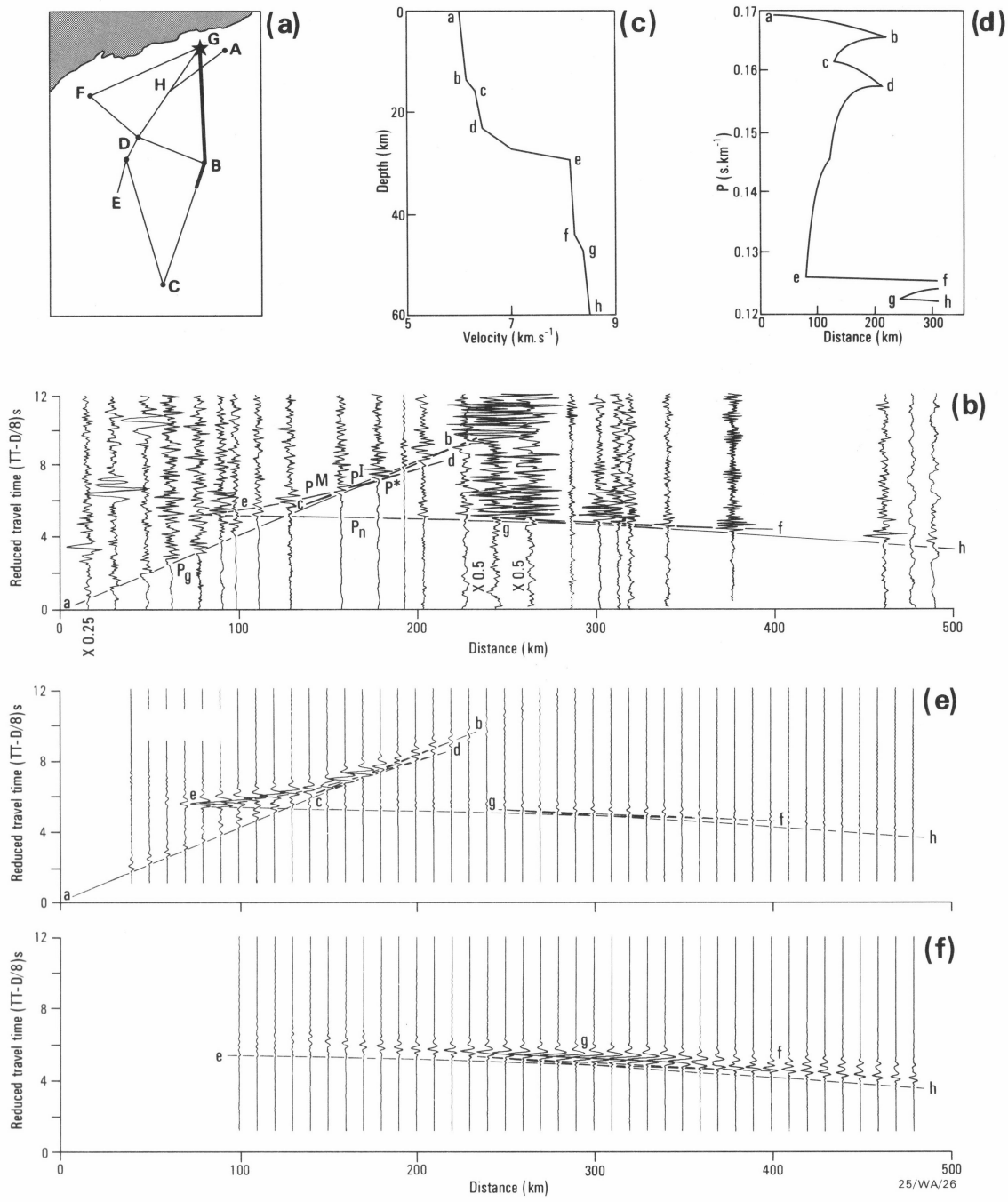

Figure 3. Model for shotpoint G (Goldsworthy), along line GBC.
(a) location diagram for the record section in Figure 3b; (b) record section southwards from G. The superimposed travel time curves are for the model in Figure 3c; (c) velocity/depth model for profile GBC; (d) p-versus-distance plot for the model in Figure 3c; (e) synthetic seismogram record section and travel-time curves for the model in Figure 3c; (f) synthetic seismogram record section for the sub-Moho phases.

quently, the interpretation of the near-surface phases is difficult, so an upper crustal model similar to that in Figure 2f was adopted for this profile.

The P^M reflection branch (de) maintains fairly large amplitudes to about 250 km. Note that the Pn arrivals (ef) are fairly small between 130 and 200 km, but beyond 200 km very large sub-Moho phases are evident. The sub-Moho arrivals have amplitudes comparable to those of the P^M phases in the same traces.

Except for the stations in about the first 100 km of the profile, the stations used in Figure 3b are the same as those used in Figure 2e for the record section of blasts at shotpoint A, in

Table 2. Velocity/depth model for the profile shotpoint G (Goldsworthy), along line GBC

Velocity (km s⁻¹)	*Depth (km)*	*Travel-time curve cusps*
6.01	0.0	a
6.15	13.0	b
6.30	15.0	c
6.45	22.0	
7.00	26.0	d
8.10	28.0	e
8.20	42.0	f
8.35	44.5	g
8.50	57.0	h

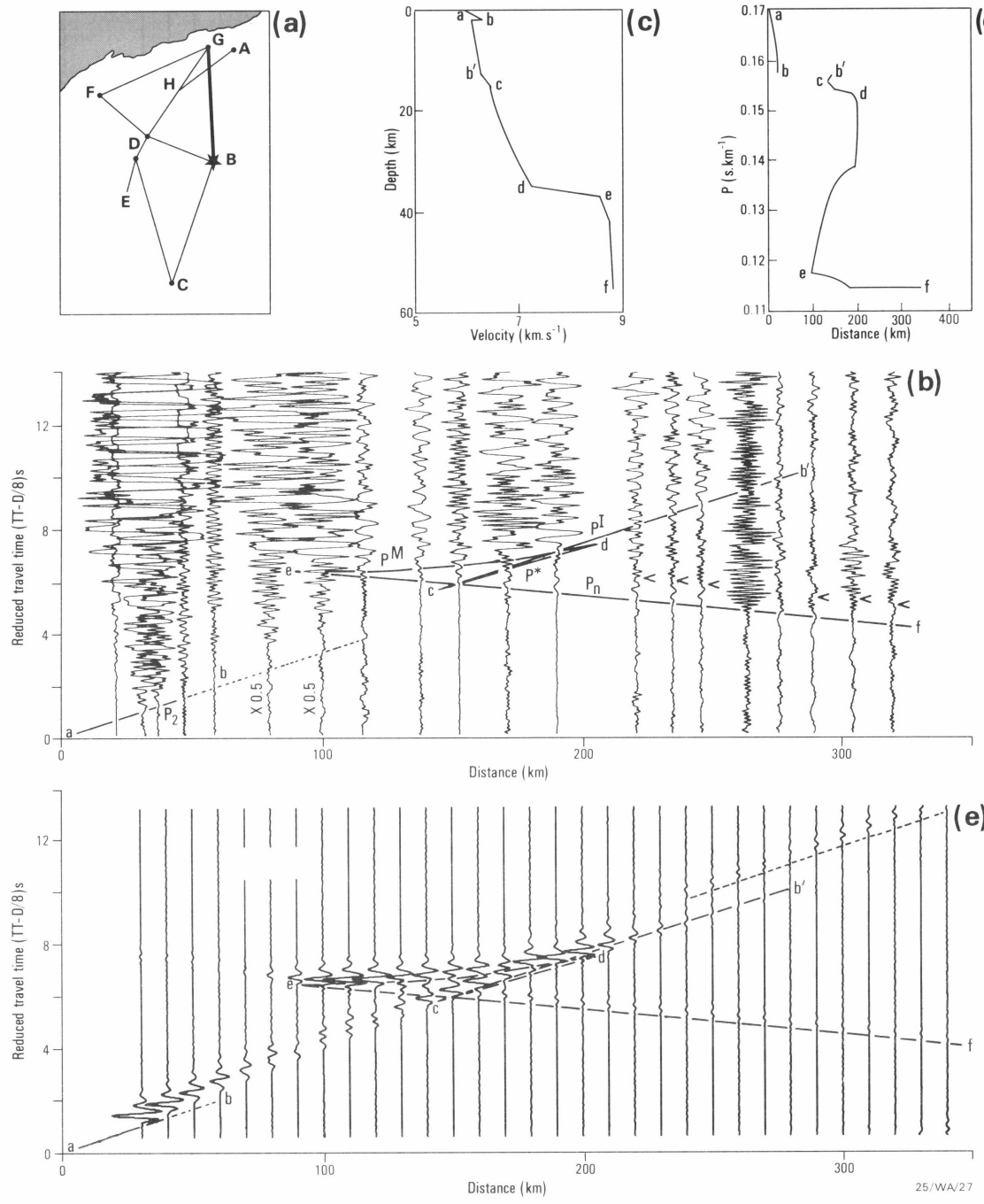

Figure 4. Model for shotpoint B (Newman), along line BG.
(a) location diagram for the record section in Figure 4b; (b) record section northwards from B. The superimposed travel-time curves are for the model in Figure 4d; (c) velocity/depth model for profile GB; (d) p-versus-distance plot for the model in Figure 4c; (e) synthetic seismogram record section and travel-time curves for the model in Figure 4c.

which only small sub-Moho phases are evident. It is, therefore, likely that source effects contributed to the large sub-Moho amplitudes in Figure 3b.

A triplication (fgh) can be interpreted in the travel-time curves at about 300 km in Figure 3b, and defines a boundary in the upper mantle about 14 km below the Moho (Fig. 3c). The triplication is probably present in Figure 2e, corresponding to the arrivals arrowed with an asterisk, but it is not clear because of small amplitudes. Figure 3f shows the amplitudes of the curves efgh in more detail than Figure 3e, in which the absolute amplitudes around the triplication fgh are similar to those of the P^M phase, as in Figure 3b.

Shotpoint B (Newman), along line BG (Fig. 4, Table 3)

The record section of blasts at shotpoint B northwards along line BG reverses the profile on Figure 3b, and differs from it in several ways.

The first arrivals along curve ab, ie. the Pg phase, are weak and emergent, probably owing to the masking effects of the near-surface, high-velocity Hamersley Basin strata. The P^M branch is very clear, with the amplitudes decaying abruptly at 200 km, forming a bright cusp. Thus, in the model (Figure 4c), the lower crust has a second-order increase of velocity with depth. This causes all the rays with ray parameters between about 0.153 and 0.138 s km^{-1}. and which bottom between 15 and

Table 3. Velocity/depth model for the profile shotpoint B (Newman), along line BG.
Note: Velocities are quoted to three decimal places only so that the second-order increase of velocity with depth between C and D is accurately defined.

	MODEL 1	
Velocity (km s^{-1})	*Depth (km)*	*Travel-time curve cusps*
5.860	0.0	a
6.350	2.0	b
6.050	2.0	
6.250	13.0	b'
6.400	15.0	c
6.475	17.0	
6.500	18.5	
6.531	20.0	
6.583	22.0	
6.645	24.0	
6.718	26.0	
6.801	28.0	
6.847	29.0	
6.895	30.0	
6.946	31.0	
7.000	32.0	
7.057	33.0	
7.116	34.0	
7.178	35.0	d
8.500	37.0	e
8.700	42.0	
8.750	55.0	

35 km to emerge between 190 and 205 km; note the broad cusp at d in the p versus distance plot in Figure 4d, and compare it with the sharp cusps at d in Figures 2g and 3d. The model gives large amplitudes at cusp d to about 200 to 210 km, after which they decay rapidly (Fig. 4e).

The Pn phase (ef) is clear, with large amplitudes. A zone of high velocity gradient (ef) below the Moho, which is transitional over 2 km, maintains the amplitudes of the Pn phase; the gradient may extend to greater depths, but the profile is too short to provide the relevant information. No triplication similar to fgh in Figure 3b can be interpreted. However, Drummond (1979a) noted that on most traces beyond 150 km a phase (arrowed) could be picked 0.6 s after the Pn arrival. The five traces beyond 250 km, are from a different blast from those between 150 and 250 km and were plotted to show that the effect is independent of the blast used. Linear regression analyses of the travel times of the two phases yielded statistically identical apparent velocities for the phases. It is possible that the second phase forms part of the triplication fgh, and its apparent velocity is rendered the same as Pn by the effects of refractor topography. Alternatively, the second arrival may be a multiple from a structure unique to the crust near shotpoint B.

The dotted travel-time curve later than and beyond b' in Figure 4e represents underside multiples from the high-velocity, near-surface layer. The data are too noisy to verify if they are observed or not.

Table 4. Velocity/depth model for the profile shotpoint G (Goldsworthy), along line GHD.
Note: Velocities are quoted to three decimal places only so that the second- order increases of velocity with depth above B and between C and D are accurately defined.

	MODEL 1	
Velocity (km s^{-1})	*Depth (km)*	*Travel-time curve cusps*
6.130	0.0	a
6.130	2.0	
6.131	3.0	
6.137	5.0	
6.142	6.0	
6.156	8.0	
6.164	9.0	
6.174	10.0	
6.185	11.0	
6.200	12.0	b
6.350	14.0	c
6.377	16.0	
6.420	18.0	
6.480	20.0	
6.515	21.0	
6.555	22.0	
6.600	23.0	
6.648	24.0	
6.700	25.0	d
8.150	29.0	e
8.250	45.0	f

Shotpoint G (Goldsworthy), along line GHD
(Fig. 5, Table 4)

The Pg phase has large, overmodulated arrivals on most traces out to the crossover distance with Pn at about 130 km. The trace at about 95 km is not overmodulated and has a clear second arrival (arrowed), interpreted as a sub-critical P^I reflection. The forward cusp d does not have any convincing arrivals beyond 180 km, where it blends with the large-amplitude P^I arrivals of the branch bc, which maintain large amplitudes to about 230 km.

The P^M phase between the forward cusp d and retrograde cusp e is clear with large amplitudes. Pn is generally weak, but is observed (arrowed, with an asterisk) on some traces between 150 and 240 km. Note that there are no large amplitudes which identify an upper mantle triplication similar to fgh observed from this shotpoint southwards along line GB in Figure 3b.

Shotpoint D (Tom Price), along line DHG (Fig. 6, Table 5)

The record section of Tom Price blasts northeast along line DHG reverses the profile of Goldsworthy blasts in Figure 5b. The record section has a gap between 100 and 180 km, across which the correlation of phases is tentative, but the correlations made seem realistic.

This record section has some of the clearest evidence of subcritical P^I reflections from the intracrustal boundary. They appear as high frequency arrivals (arrowed) up to a second after Pg in the four traces between 60 and about 100 km.

The P^M phase must be correlated across the gap in the recordings. Strong arrivals are observed at cusp d, at about 240 km, beyond which they decay rapidly. The Pn phase is weak, although some arrivals (arrowed, with an asterisk) may be identified.

Table 5. Velocity/depth model for the profile shotpoint D (Tom Price), along line DHG.
Note: Velocities are quoted to three decimal places only so that the second- order increase of velocity with depth between C and D is accurately defined.

Velocity (km s^{-1})	*Depth (km)*	*Travel-time curve cusps*
6.100	0.0	a
6.250	11.5	b
6.400	14.5	c
6.500	18.0	
6.520	20.0	
6.550	22.0	
6.589	24.0	
6.638	26.0	
6.696	28.0	
6.728	29.0	d
8.150	34.0	e
8.250	50.0	f

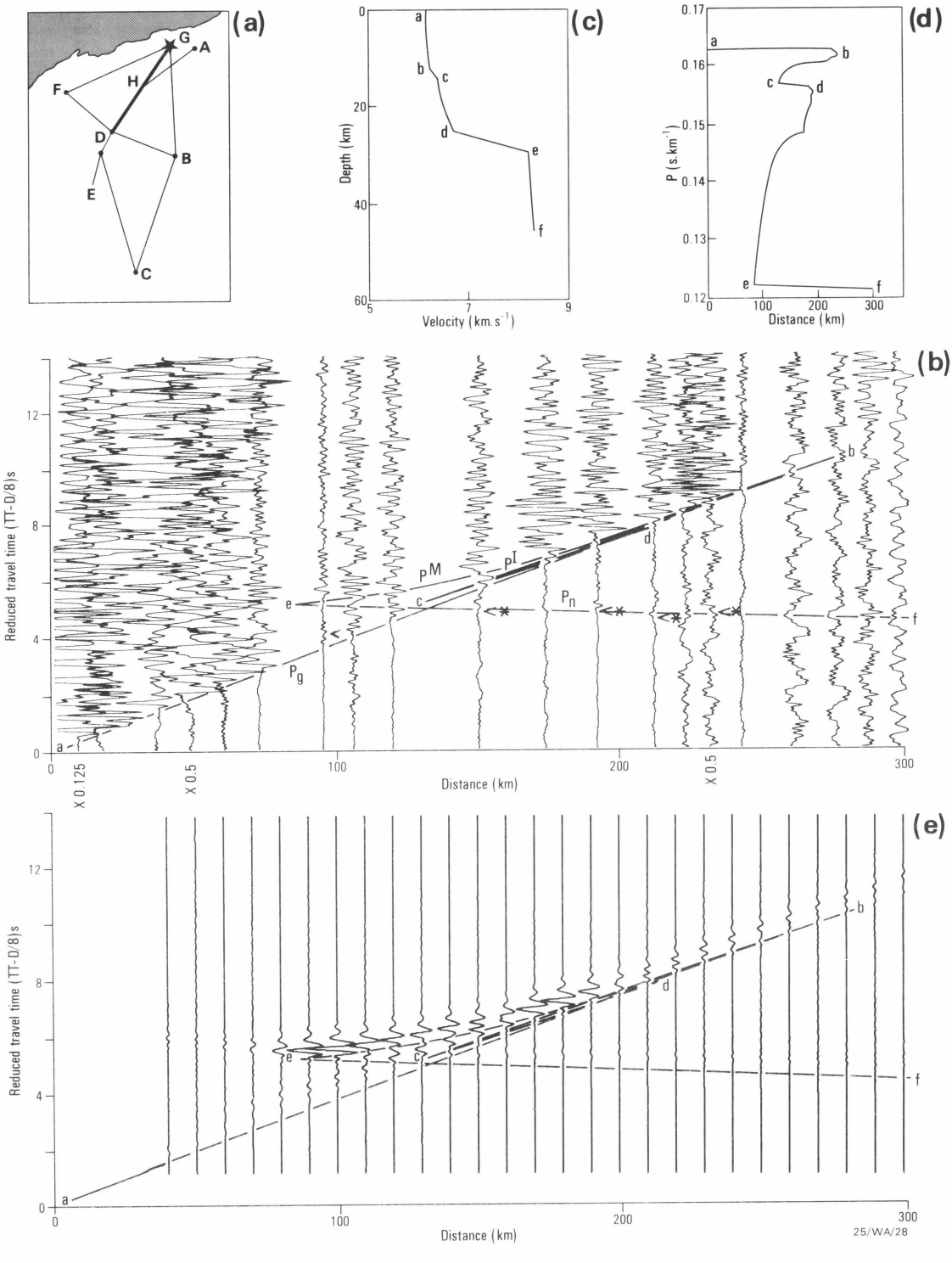

Figure 5. Model for shotpoint G (Goldsworthy), along line GHD.
(a) location diagram for the record section in Figure 5b; (b) record section southwards from G. The superimposed travel-time curves are for the model in Figure 5c; (c) velocity/depth model for profile GHD. (d) p versus distance plot for the model in Figure 5c; (e) synthetic seismogram record section and travel-time curves for the model in Figure 5c.

Shotpoint D (Paraburdoo), along line DHG (Fig. 7, Table 6)

The Pg phase, where observed, decays rapidly near the blast, probably because of the near-surface high-velocity Hamersley Basin rocks at the southern end of the profile (Drummond, 1981). The high-velocity layer extends about 60 km north of Paraburdoo and does not affect the up-going rays for most of this profile.

The intracrustal boundary must be included in the model, because this profile duplicates much of that included in Figure 6b, where very clear subcritical reflections off the boundary were noted, but there is very little evidence for the boundary in this record section at this scale. The boundary is modelled (Fig. 7c, Table 6) as very gradational, with velocity gradients above and below to cause only a small triplication cd.

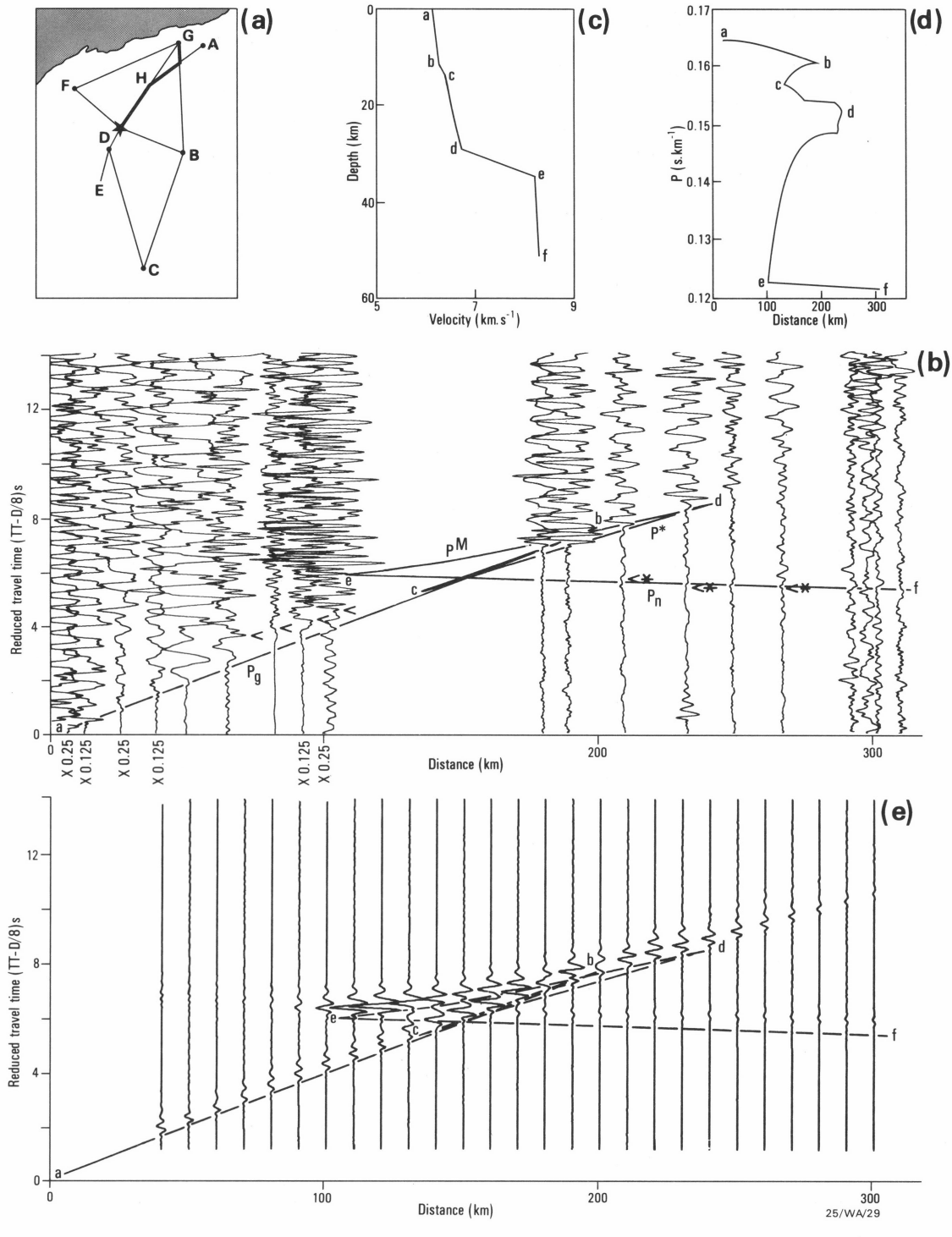

Figure 6. Model for shotpoint D (Tom Price), along line DHG.
(a) location diagram for the record section in Figure 6b; (b) record section northwards from Tom Price, at D. The superimposed travel time curves are for the model in Figure 6c; (c) velocity/depth model for profile DHG, from blasts at Tom Price; (d) p-versus-distance plot for the model in Figure 6c; (e) synthetic seismogram record section and travel-time curves for the model in Figure 6c.

Shotpoint F (Pannawonica), along line FDB (Fig. 8, Table 7)

The blast used to construct the record section from 190 to 370 km was large, dispersed over several kilometres, and had a burning time of 2.17 s. Consequently, the seismic energy from the blast is not a clear, sharp pulse, but an oscillating, high frequency wavelet of over one second duration, and secondary arrivals buried in the coda of previous phases are not easy to distinguish on all traces beyond 190 km. The forward cusps b and d are difficult to identify, but they are interpreted at about 220 and 250 km, respectively. The Pn phase ef has a low apparent velocity (7.6 km s^{-1}), but high amplitude arrivals, compared to Pn on other profiles.

The model for the profile is shown in Figure 8c and Table 7; the synthetic seismogram record section for the model is illustrated in Figure 8e.

Several large amplitude phases are observed as later arrivals beyond 190 km in Figure 8b. They have apparent velocities

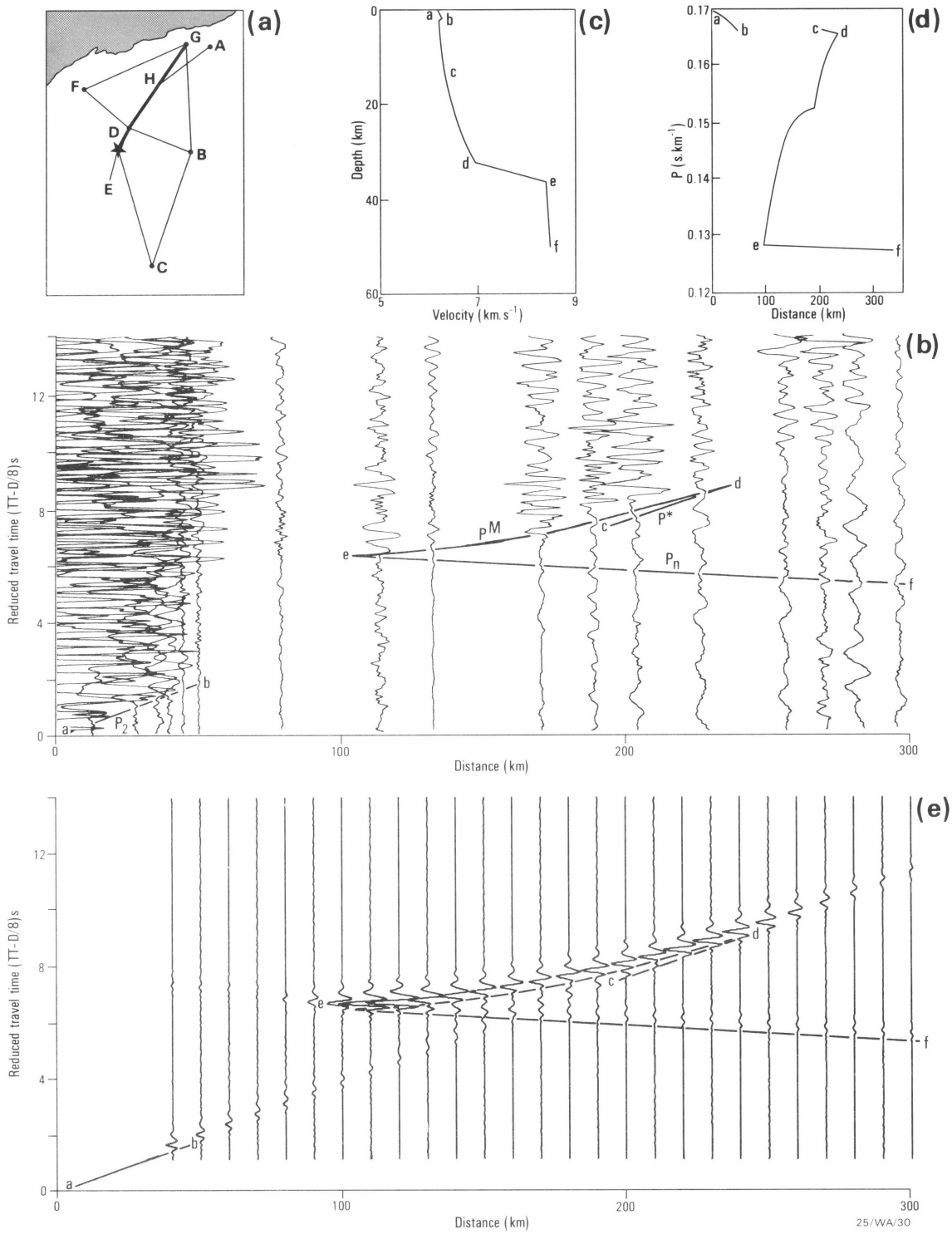

Figure 7. Model for shotpoint D (Paraburdoo), along line DHG.
(a) location diagram for the record section in Figure 7b; (b) record section northwards from Paraburdoo, at D. The superimposed travel-time curves are for the model in Figure 7c; (c) velocity/depth model for profile DHG, from blasts at Paraburdoo; (d) p-versus-distance plot for the model in Figure 7c; (e) synthetic seismogram record section and travel time curves for the model in Figure 7c.

similar to that of the Pg phase, and are similar to multiples from the lower crust recorded in Canada by Mereu & others (1977).

Mereu & others (1977) interpreted their multiples as phases focussed at the surface by strong gradients in the lower crust and then internally reflected at the free surface. However, rays will be internally reflected at the free surface only if the angle of incidence is small, and in Mereu & others' (1977) model this was achieved by including low-velocity sediments in the model. However, the Hamersley Basin strata have higher velocities than the basement, and rays internally reflected to emerge as multiples within 200 to 400 km of the blast would have to have angles of incidence at the free surface greater than 50 degrees. These would not be internally reflected at the free surface. However, energy incident at the base of the Hamersley Basin strata would be partitioned into both transmitted and reflected energy. The transmitted energy would reach the surface as primary waves, and the reflected energy would

Table 6. Velocity/depth model for the profile shotpoint D (Paraburdoo), along line DHG.
Note: Velocities are quoted to three decimal places only, so that the second- order increases of velocity with depth above C and between C and D are accurately defined.

Velocity (km s^{-1})	*Depth (km)*	*Travel-time curve cusps*
6.190	0.0	a
6.300	2.0	b
6.190	2.0	
6.200	8.0	
6.209	9.0	
6.219	10.0	
6.230	11.0	
6.300	14.0	c
6.325	16.0	
6.360	18.0	
6.406	20.0	
6.462	22.0	
6.529	24.0	
6.606	26.0	
6.648	27.0	
6.693	28.0	
6.741	29.0	
6.791	30.0	
6.844	31.0	
6.900	32.0	d
8.350	36.0	e
8.450	50.0	f

return to the surface as multiples at greater distances. The amplitudes of the multiples will be dependent on the degree of partitioning, which, in turn, depends on the angle of incidence, the velocity in the basement, and the velocity in the basin strata. The angle of incidence will in turn be affected by topography of the interface between the basin strata and the basement; the velocity in the basement has to be assumed for part of this profile; and the velocity in the basin strata changes along the profile (Drummond & others, 1981). Thus, to try to model the amplitudes of the multiples with a program that allows only laterally homogeneous models would be fruitless.

The travel-time curves with the crosses and the dots are the times of the multiples off the intracrustal boundary and the Moho, respectively, reflected off the underside of the high-velocity layer, assuming that the velocity in the high-velocity layer at the point of reflection approximately half-way along the profile is 6.3 km s^{-1} (Drummond & others, 1981), and that the layer is 2 km thick, and are in reasonable agreement with the observed times.

Shotpoint B (Newman), along line BDF (Fig. 9)

The record section (Fig. 9b) has a very high (6.65 km s^{-1}) velocity branch (ab) near the source. The large amplitudes of branch ab, which is the P_2 phase of Drummond & others (1981)

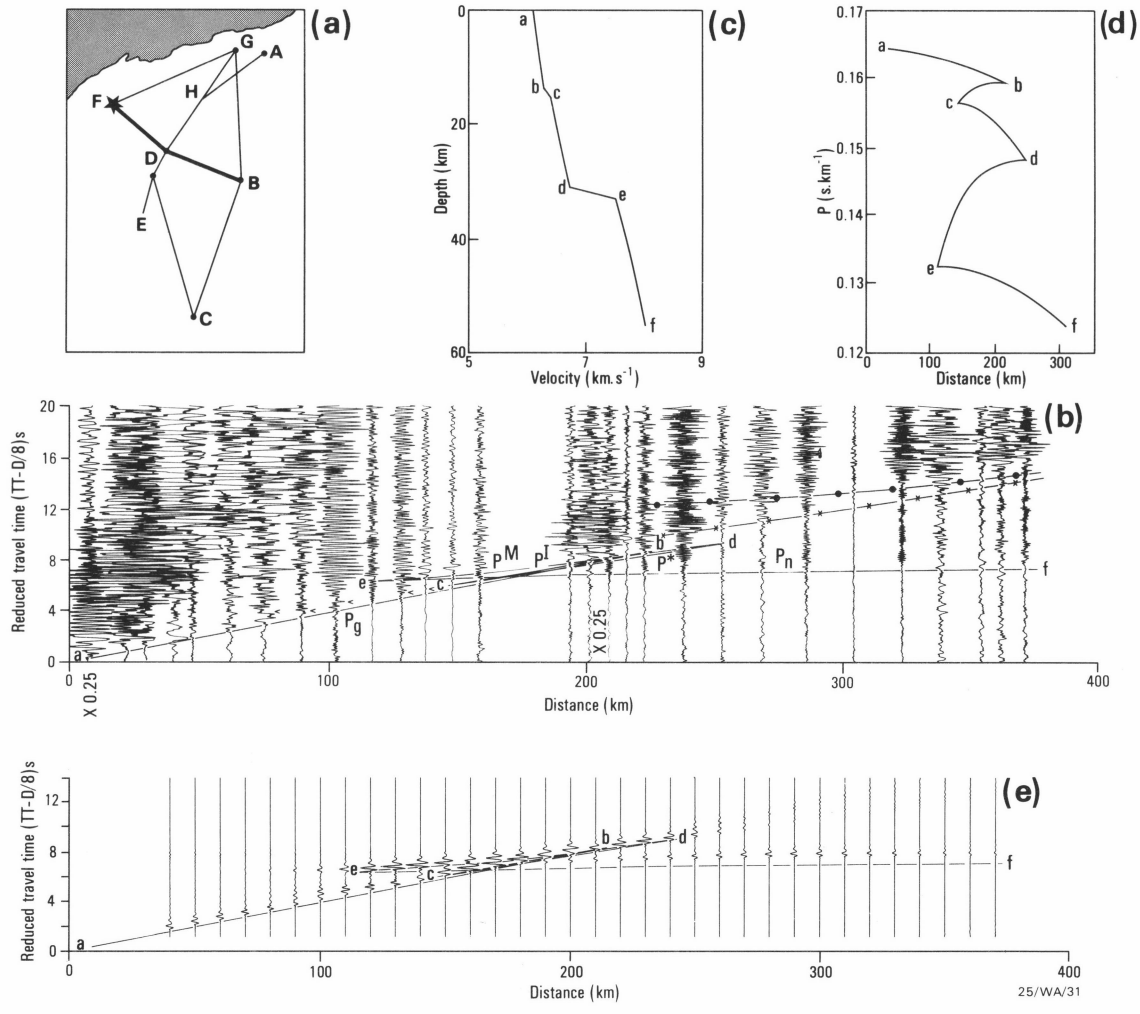

Figure 8. Model for shotpoint F (Pannawonica), along line FDB.
(a) location diagram for the record section in Figure 8b; (b) record section southeastwards from F. The superimposed travel-time curves are for the model in Figure 8c; (c) velocity/depth model for profile FDB. (d) p-versus-distance plot for the model in Figure 8c; (e) synthetic seismogram record section and travel-time curves for the model in Figure 4c.

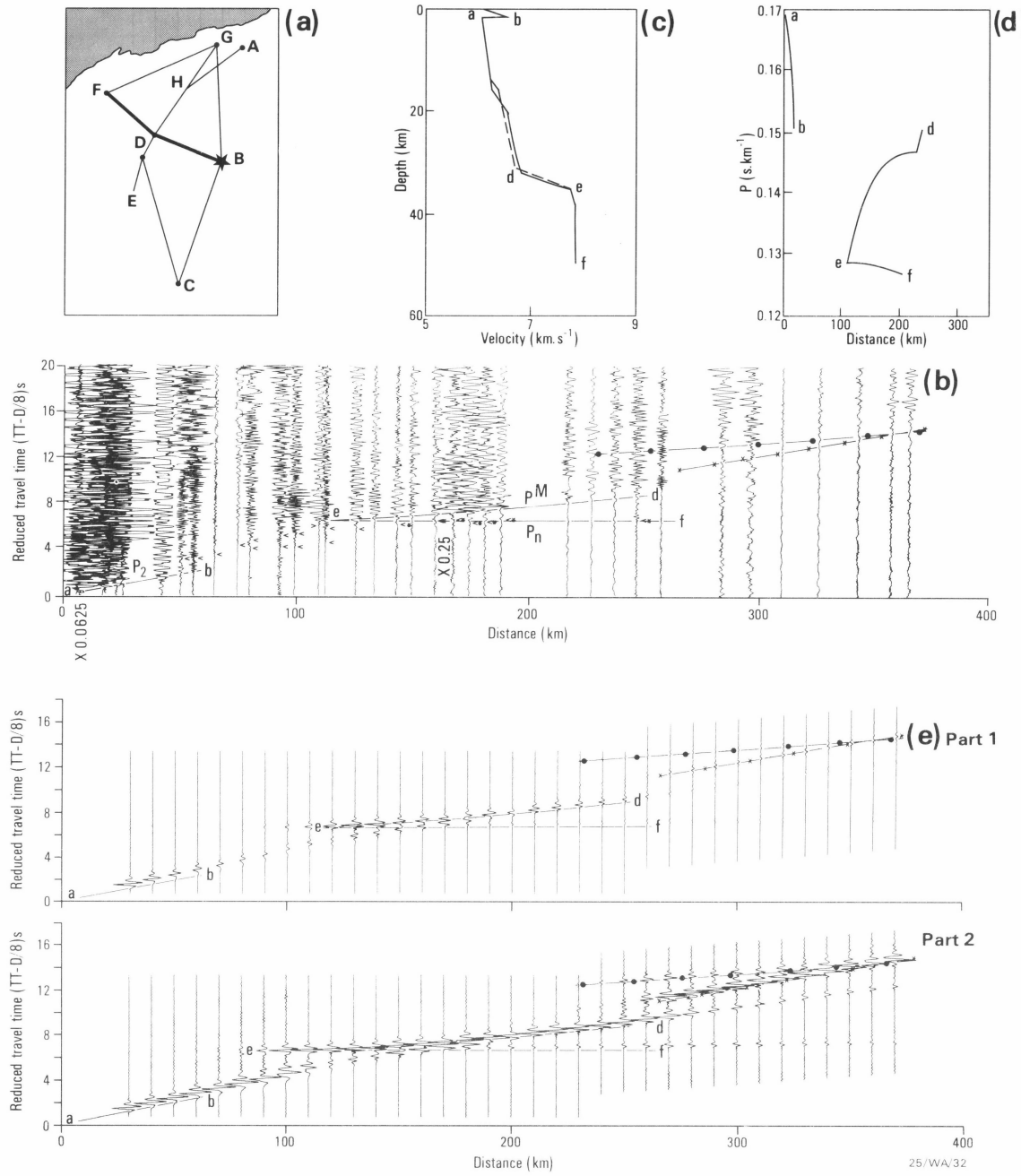

Figure 9. Models for shotpoint B (Newman), along line BDF.
(a) location diagram for the record section in Figure 9b; (b) record section northwestwards from B. The superimposed travel-time curves are for the model drawn with the solid line in Figure 9c. Those marked with dots indicate the first multiple from the Moho, and those marked with crosses, the first multiple from the intracrustal boundary, reflected as underside reflections from the near-surface, high-velocity layer; (c) Model 1 (solid curve) and Model 2 (dotted curve) for profile BDF; (d) p versus distance plot for Model 1 in Figure 9c; (e) synthetic seismogram record section and travel-time curves for Model 1 in Figure 9c. The multiples are as for Figure 9b. Part 1: amplitudes relative to the largest overall peak to trough amplitude, Part 2: trace normalised, so that the maximum peak to trough amplitude is the same for all traces.

Table 7. Velocity/depth model for the profile shotpoint F (Pannawonica), along line FDB.

Velocity (km s^{-1})	*Depth (km)*	*Travel-time curve cusps*
6.07	0.0	a
6.25	14.0	b
6.37	16.0	c
6.70	31.0	d
7.50	33.0	e
8.00	55.0	f

and Drummond (1981), decay rapidly beyond 50 km, and imply a near-surface high-velocity layer overlying a basement with a lower velocity.

The Pg, P^I and P* phases are difficult to identify in the record section. While the near-surface, high-velocity layer might be expected to mask out all of the effects of the upper crust, the P_2 phase velocity decreases to the northwest, and the high-velocity layer pinches out in places against basement domes, so that there are windows in the high-velocity layer through which the crustal phases can reach the surface. Such arrivals can be

Table 8. Velocity/depth models for the profile shotpoint B (Newman), along line BDF.
Note: In Model 1, velocities are quoted to three decimal places only so that the second-order increase of velocity with depth above D is accurately defined.

MODEL 1			MODEL 2		
Velocity (km s^{-1})	*Depth (km)*	*Travel-time curve cusps*	*Velocity (km s^{-1})*	*Depth (km)*	*Travel-time curve cusps*
5.950	0.0	a	5.90	0.0	a
6.650	2.0	b	6.65	2.0	b
6.050	2.0		6.10	2.0	
6.250	16.0		6.25	14.0	
6.550	20.0		6.37	16.0	
6.565	22.0		6.70	31.0	d
6.591	24.0		7.75	35.0	e
6.627	26.0		7.85	39.0	f
6.674	28.0	d	7.85	50.0	
6.732	30.0				
6.800	32.0	e			
7.750	35.0				
7.850	39.0	f			
7.850	50.0				

seen (arrowed) between 60 and 140 km in Figure 9b, although correlation between them is difficult.

The P^M phase (de) has large amplitudes which decay abruptly beyond cusp D at 260 km. The Pn phase is observed on some traces (arrowed, with an asterisk, in Fig. 9b) to 250 km, beyond which it is not observed.

Because of the screening effect of the near-surface, high-velocity layer, it is not possible to derive a unique model of the crust from this record section, so two models are presented. Many others would fit the data equally as well.

Model 1 is presented as a solid curve in Figure 9c and listed in Table 8, and is based on the model in Figure 4c for the record section for the same shotpoint to the north along line BG, although some changes were necessary to account for different apparent velocities of the phases ab, de, and ef, and their intercept times.

The synthetic seismogram record section in Figure 9e has multiples from the intracrustal boundary and the Moho. They are especially evident on the trace-normalised synthetic seismogram record section (Figure 9e, part 2) and correlate with a band of recorded arrivals which have considerable energy (Figure 9b). They are similar to those noted in Figure 8b for the reversed profile from shotpoint F.

Model 2 for this profile, presented in Figure 9c as a dotted curve and listed in Table 8, is based on the model for the reversed profile from shotpoint B (Fig. 8). The high-velocity, near-surface layer has been included, and the structure at and below the Moho changed to suit the apparent velocity and amplitudes of the Pn phase. It is not possible on the basis of the present data to give preference to either Model 1 or Model 2 for this profile. Both are based on models from other profiles in the region, and both fit the data for this profile equally well.

Bright cusps caused by lateral structure

Mereu (1969) showed that topography on a boundary can cause amplitude changes, and even triplications, along travel-time branches. Caution was expressed above that the velocity/depth models derived by synthetic seismogram modelling would be valid only if the effects of vertical structure overprinted the effects of lateral structure. The purpose of this section is to examine briefly whether the bright cusps interpreted in Figures 4, 5, 6, and 7 could be caused by the effects of lateral structure.

In all profiles, the bright cusps occur at about 200 km. If the energy which is focussed at these bright cusps is assumed to bottom halfway between the shotpoints and the recorded distances of the bright cusps, the bottoming points must be about 100 km from the shotpoints. In all but Figure 5, this would mean that the bottoming point of the rays was near the axis of the Hamersley Basin. This corresponds to a basin-shaped depression in the intracrustal boundary (Drummond, 1981). While no comparable basin-shaped depression has been interpreted at the crust/mantle boundary, a topography of 1 or 2 km would be within the error limits of the intercept method interpretation.

Figure 10 explores empirically the effects of refractor topography on the concentration of seismic rays at the surface. It must be stressed that while the model in Figure 10 is based loosely on the model of Drummond (1981) for line DHG, no attempt was made to accurately model the travel-times. The topography on the intracrustal boundary is that interpreted by Drummond (1981). The Moho dips from 28 km in the north (right hand end) to 32 km in the south (left hand end), and has superimposed on it a sinusoidal-type topography with an amplitude of less than 2 km and a wavelength of 70 km. It is represented by straight line segments 10 km long. The upper and lower crusts have velocity gradients from 6.0 to 6.15 km s^{-1} and 6.35 to 6.65 km s^{-1}, respectively; these are typical of the gradients of the velocity/depth models above (without the second order increase of velocity with depth required to cause the bright cusps). First order discontinuities were used between the layers.

Only the ray paths for mantle reflections are shown. Those which bottom between A and B, where there is no reflector topography, emerge at the surface between A' and B'. Note that the distance between A' and B' is greater than that between A and B. Rays which bottom between C and D, where the reflecting surface is concave upwards, emerge between C' and D', and because the distance from C' to D' is less than that between C and D, there is some focussing of the seismic energy. This can be seen in some cases where rays which impinge on different straight line segments of the interface emerge at almost the same point at the surface. Rays which strike the reflector between E and F, where the surface is concave downwards, are scattered and emerge between E' and F', and because E'F' is very much greater than EF, there will be a sudden diminution of amplitudes of the reflected waves beyond D'.

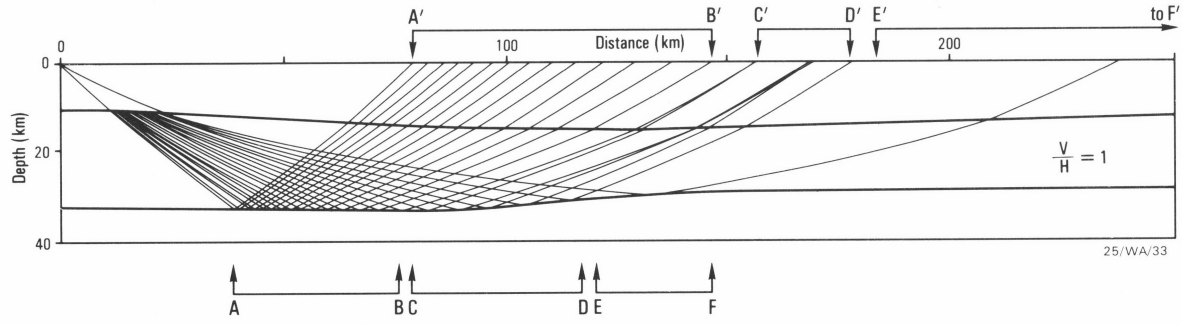

Figure 10. An example of how reflector topography can produce bright cusps.
The model is based loosely on the model for line GHD (Drummond, 1981).

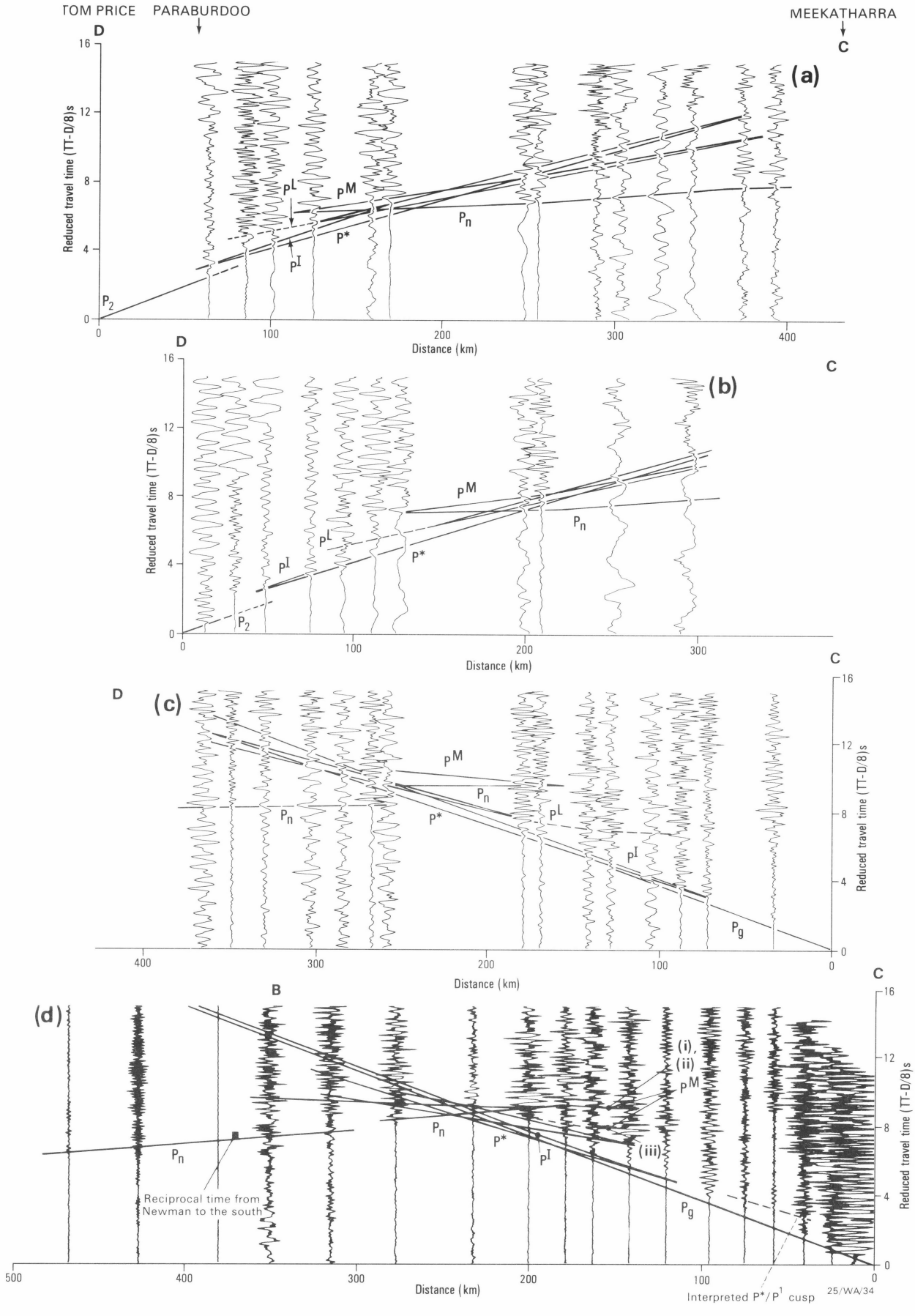

Figure 11. Record sections across the Capricorn Orogen, comparing the positions of the observed P^L and P^I/P^* cusps with the positions of those from the models of the intercept method interpretation.
Parts a, b & c are from Drummond (1981); part d is from Drummond (1979a).

Other models could be found to demonstrate the focussing effects of the reflector between C and D. Figure 10 illustrates that focussing can be caused by structures which are concave towards the energy source, and scattering of the energy will be caused by structures which are convex towards the energy source.

No preference can be given to models with either vertical or lateral structure. In the velocity/depth models from the amplitude studies, the second-order increases of velocity with depth used to produce the bright cusps have little effect on the depths of the seismic boundaries, and the refractor topography required to produce bright cusps in the regions where there are no such second-order increases is very small. Thus the velocity/depth models from the amplitude studies are likely to be good approximations of the velocity/depth functions in the Earth, regardless of whether the bright cusps are caused by lateral or vertical structure (or both).

Observed amplitudes in the Capricorn Orogen.

Current synthetic seismogram techniques are not applicable in the Capricorn Orogen (lines BC and DC), because the crust in the orogen is not laterally homogeneous (Drummond, 1981). However, some observations can be made about the nature of the boundaries, based on the fit to the observed data of the ray-theoretical cusps derived using models from the intercept method of interpretation (Drummond, 1979a; 1981).

Drummond (1981) noted that the P^L phase, assumed to be reflections from a lower crustal layer in the Capricorn Orogen and the northern Yilgarn Craton, occurred much closer to the blast than expected from ray theory (Fig. 11a, 11b and 11c). Similarly, Drummond (1979b) noted that the sub-critical reflections at the P^*/P^I cusp on line CB (dashed in Fig. 4d) were quite large. They are observed within 40 km of the blast, whereas the ray-theoretical cusp falls at about 120 km.

The large amplitudes of the sub-critical phases mean that either the boundaries are sharp, and/or low-velocity zones exist within the crust and the boundaries are, therefore, much shallower than interpreted. With the current data, it is not possible to distinguish between these alternatives, although low-velocity channels extensive enough to halve the critical distance would seem unlikely to be caused by thermal effects in such a geothermally cold region (Cull & Denham, 1979), and changes of lithology are more likely causes. However,the travel times of P^M phases (Drummond, 1979a), and the gravity field (Wellman, 1978; Drummond & Shelley, 1981) both suggest that, in the Capricorn Orogen, the lower crust must have steep velocity (and density?) gradients, and not low velocity (and density) channels. Thus, the crust in the Capricorn Orogen is unlikely to be any thinner than modelled by Drummond (1979b; 1981).

Discussion

The seismic velocity/depth models for the Pilbara Craton (Fig. 2–9, Tables 1–8) all have a two-layered crust (excluding the near-surface high-velocity Hamersley Basin strata in some of the models). Within the crustal layers, the velocity varies from about 6.0 km s^{-1} at the surface to about 6.2 km s^{-1} just above the intracrustal boundary, and from about 6.4 km s^{-1}. just below the intracrustal boundary to between 6.6 and 7.2 km s^{-1} at the base of the crust, which is from 28 to 37 km thick. The intracrustal boundary is transitional over 2–3 km depth, and the Moho is transitional over 2–5 km. Apparent velocities in the uppermost mantle vary from 7.5 to 8.5 km s^{-1}. On one profile, a sub-Moho discontinuity was noted 14 km below the Moho. The crust/mantle boundary dips southwards across the Pilbara Craton (Drummond, 1979a). The highest apparent Pn velocities, the highest apparent velocities in the lowermost crust, and the thickest crust were all interpreted on northerly trending up-dip profiles. The models with the thinnest crust were interpreted on the profiles that trended southwards from the northern shotpoints under which the Moho is shallowest. Thus many of the variations in apparent Pn velocity, crustal velocities, and crustal thickness are caused by the effects of dip on the crust/mantle boundary. However, not all of the differences in apparent Pn velocity can be explained by the effects of refractor dip. The lowest apparent Pn velocities were not observed in the direction of down-dip on the crust/mantle boundary, but along the axis of the Hamersley Basin, which parallels the strike of the crust/mantle boundary. This was noted before by Drummond & others (1981), who suggested that the seismic velocities in the upper mantle were lower along the axis of the basin either because of the effects of metamorphism or partial melting (removal of iron), or because they were exhibiting anisotropy.

The velocity/depth models in Figures 2 to 9 all have slightly thicker crusts than those in the models of Drummond (1979a; 1981) and Drummond & others (1981), but the differences are less than about 10 percent. In the new models, the crust in the Pilbara Craton is still thinner, especially when the effects of refractor dip are considered, than in the previous models for the Capricorn Orogen, where positive velocity gradients are still preferred. The crust in the original models of the Yilgarn Craton was more than 50 km thick. No evidence is available to suggest that massive low-velocity channels exist within the crust of the Yilgarn Craton, and it is reasonable to suggest that increasing metamorphic grade with depth will increase the velocity with depth through the crustal layers. This will have the effect of increasing the crustal thickness in the models. Thus, Drummond's (1981) assumptions about the relative thicknesses of the crust from the Pilbara Craton southwards across the Capricorn Orogen to the Yilgarn Craton are justified, and the implications that the changes in crustal thickness have for tectonic evolutionary models of the region still hold.

Acknowledgements

The work described in this paper forms part of a study of northwest Australia undertaken while I was a research scholar at the Research School of Earth Sciences, Australian National University, under the auspices of an Australian Public Service Postgraduate Scholarship. K.J. Muirhead and C. Wright of RSES made useful comments and read an early draft of the manuscript. D.M. Finlayson and D. Denham also provided advice. The computer program REFLEXION was made available by Prof. K. Fuchs, and J. Leven and G. Bock modified it and converted it to the RSES computer. C.D.N. Collins also provided computing advice.

References

Aki, K., & Richards, P.G., 1980 — Quantitative seismology, Volume 1. *W.H. Freeman & Company.*

Berry, M.J., 1971 — Depth uncertainties from seismic first-arrival refraction studies. *Journal of Geophysical Research*, 76, 6464–6468.

Berry, M.J., & Fuchs, K., 1973 — Crustal structure of the Superior and Grenville Provinces of the northeastern Canadian shield. *Seismological Society of America, Bulletin*, 63, 1393–1432.

Braile, L.W., & Smith, R.B., 1975 — Guide to the interpretation of crustal refraction profiles. *Geophysical Journal of the Royal Astronomical Society*, 40, 145–176.

Bullen, K.E., 1960 — Note on cusps in seismic travel times. *Geophysical Journal of the Royal Astronomical Society*, 3, 354–359.

Cull, J.P., & Denham, D., 1979 — Regional variations in Australian heat flow. *BMR Journal of Australian Geology & Geophysics*, 4, 1–13.

Drummond, B.J., 1979a — A crustal profile across the Archaean Pilbara and northern Yilgarn Cratons, northwest Australia. *BMR Journal of Australian Geology & Geophysics*, 4, 171–180.

Drummond, B.J., 1979b — Pilbara crustal survey, 1977: operational report. *Bureau of Mineral Resources, Australia, Record*, 1979/54 (unpublished).

Drummond, B.J., 1981 — Crustal structure of the Precambrian terrains of north-west Australia from seismic refraction data. *BMR Journal of Australian Geology & Geophysics*, 6, 123–135.

Drummond, B.J., in preparation — Seismic constraints on the chemical composition of the Pilbara Craton, northwest Australia. *Submitted to the Proceedings of the International Symposium of Archaean and early Proterozoic Geologic Evolution and Metallogenesis, Salvador, Brazil, 1982.*

Drummond, B.J., & Shelley, H.M., 1981 — Isostasy and structure of the lowercrust and upper mantle in the Precambrian terrains of northwest Australia. *BMR Journal of Australian Geology & Geophysics*, 6, 137–143.

Drummond, B.J., Smith, R.E., & Horwitz, R.C., 1981 — Crustal structure in the Pilbara and northern Yilgarn Blocks from deep seismic sounding. *In* Glover, J.E., & Groves, D.I. (editors), Archaean geology. *Second International Archaean Symposium. Geological Society of Australia, Special Publication*, 7, 33–41.

Finlayson, D.M., Collins, C.D.N., & Denham, D., 1980 — Crustal structure under the Lachlan Fold Belt, southeastern Australia. *Physics of the Earth and Planetary Interiors*, 21, 321–342.

Fuchs, K., 1968 — Das Reflexions und Transmissionsvermogen eines geschichteten Mediums mit beliebiger Tiefen–Verteilung der elastischen Moduln und der Dichte fur schragen Einfall ebener Wellen. *Journal of Geophysics*, 34, 389–413. English translation by Feeken, E.H., 1979 — The reflectivity and transmittance of a stratified medium with variable depth distribution of moduli of elasticity and density for inclined incidence of plane waves. *In* Collins, C.D.N., 1979 — Adaption of the synthetic seismogram program 'REFLEX' to the CSIRO CYBER 76 computer. *Bureau of Mineral Resources, Australia, Record*, 1979/7 (unpublished).

Fuchs K., & Muller, G., 1971, — Computation of synthetic seismograms with the reflectivity method and comparison with observations. *Geophysical Journal of the Royal Astronomical Society*, 23, 417–433.

Gee, R.D., 1979 — Tectonics of the Western Australian shield. *Tectonophysics*, 50, 327–369.

Kind, R., 1976 — Computation of reflection coefficients for layered media. *Journal of Geophysics*, 41, 191–200.

Mereu, R.F., 1969 — Effect of Mohorovicic topography on the amplitude of seismic P waves. *Journal of Geophysical Research*, 74, 4371–4376.

Mereu, R.F., Majumdar, S.C., & White, R.E., 1977 — The structure of the crust and upper mantle under the highest ranges of the Canadian Rockies from a seismic refraction survey. *Canadian Journal of Earth Sciences*, 14, 196–208.

Mueller, S., & Landisman, M., 1966 — Seismic studies of the earth's crust in continents. I: Evidence for a low-velocity zone in the upper part of the lithosphere. *Geophysical Journal of the Royal Astronomical Society*, 10, 525–538.

Mueller, S., & Landisman, M., 1971 — An example of the unified method of interpretation for crustal seismic data. *Geophysical Journal of the Royal Astronomical Society*, 23, 365–371.

Wellman, P., 1978 — Gravity evidence for abrupt changes in mean crustal density at the junction of Australian crustal blocks. *BMR Journal of Australian Geology & Geophysics*, 3, 153–162.